Fiber-Optic Vector Magnetic Field Sensor Based on Mode Interference and Magnetic Fluid in a Two-Channel Tapered Structure

He Tian
Yuxiao Song
Yanzeng Li
Hanyang Li
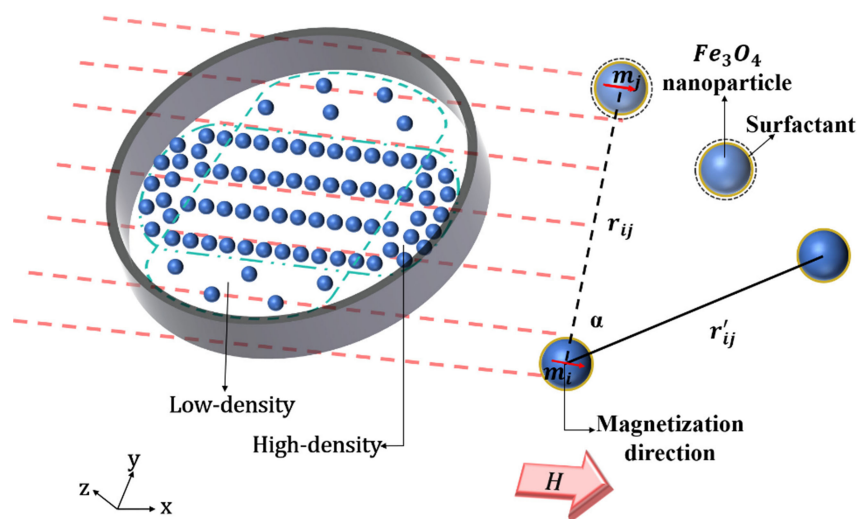
IEEE

Fiber-Optic Vector Magnetic Field Sensor Based on Mode Interference and Magnetic Fluid in a Two-Channel Tapered Structure

He Tian [ID],[1] **Yuxiao Song** [ID],[2] **Yanzeng Li**,[3] **and Hanyang Li** [ID] [2,3]

[1]College of Science, Northeast Forestry University, Harbin 150040, China
[2]Key Lab of In-fiber Integrated Optics, Ministry Education of China, Harbin Engineering University, Harbin 150080, China
[3]Department of Physics and Optical Science, University of North Charalotte, Charelotte, North Carolina 28223-0001 USA

Abstract: An innovative approach to high-sensitivity simultaneous intensity and direction measurement in a two-channel tapered sensor is proposed and demonstrated. The sensor is comprised of magnetic fluid (MF)- filled micro-capillary and two accompanying micro-fiber, thus enabling evanescent interaction to take place between the optical mode in the capillary and MF. Given the magnetic nanoparticles (MNPs) of MF manifest anisotropic magnetic field. Experimental and numerical simulations were performed simultaneously, which provided a better understanding of the interaction between light and MF in addition to clarifying the dynamic process of MNPs within MF with the assistance of varying magnetic field. The experimental results are well consistent with the numerical simulation results and show that the sensitivity of this sensor reaches up to 244 pm/mT, with the direction error being merely $\pm 1.4°$. Therefore, the proposed sensor exhibits a unique sensitivity for the measurement of magnetic field intensity and direction in 3D space, which makes it best suitable for applications in transportation, medicine, and smart device.

Index Terms: Magnetic field sensor, magnetic fluid, fiber optics sensors.

1. Introduction

Magnetic field sensor is extensively applicable to various industries or purposes such as aerospace, environmental monitoring, navigation, energy survey and so on [1]. When the environment is severely polluted or overly harsh, the performance of conventional electromagnetic sensors will be subject to serious impact. It even breaks down in some extreme cases. Due to its simple structure and resistance to electromagnetic interference from external components, the fiber-optic magnetic field sensor is made suited to the hazardous environment where the use of electricity is banned [2]. Normally, the initial fiber structure needs to be combined with some functional materials to achieve magnetic field measurement. For instance, Terfenol-D, TbDyFe and magnetic fluid (MF) [3]–[5]. Among a wide range of functional materials, the magnetic fluid (MF), consisting of colloidal magnetic nanoparticles and surfactants interspersed in a suitable carrier liquid, is a special magnetic material with liquid fluidity which has been commonly used in magnetic field measurements [6].

In addition to the excellent physical property, MF presents versatile magneto-optical properties including tunable effective refractive index (ERI), tunable transmission loss and birefringence [6]–[9], which indicate a huge potential application in the design of magnetic field sensors. In previous works, the sensors combined with MF have been primarily designed into MF coating-based [10]–[19] and MF filling-based [9], [20]–[23] structures. With MF acting as the modified cladding, various kinds of MF coating-based magnetic field sensors have been designed, such as grating-based sensors [15]–[17], interferometric based sensors [7], [10]–[12], and other sensing schemes [13]–[18]. In addition, considering the tunability of RI, the MF filling-based sensors can be realized by injecting MF into the air-hole of photonic crystal fibers (PCF) or the cavity of microstructure fibers [9], [20]–[23]. Recently, the fiber-optic vector magnetic field sensors have been reported as a good candidate for measuring both magnetic field intensity and direction simultaneously [15], [18], [24], yet there is a lack of evidence illustrating the directional detection for the magnetic field. For instance, a vector magnetic field sensor, based on the integration of a side-polished-fiber (SPF)-based surface plasmon resonance (SPR) structure with MF [25], was merely studied by its high sensitivity (598.7 pm/Oe) to the magnetic field intensity, not including the effect of changing the sensor axis. Besides, SPR-based devices typically require a vacuum coating process, and the material and thickness of the coating layer are important factors to be considered. Another proposed optical fiber vector magnetometer was fabricated by fully injecting MF into the micro-channels array of the double-cladding PCF [26]. Compared to the other MF-based optical fiber magnetic field sensors this magnetometer has some inherent advantages in well robustness and orientation determinations. However, both the injection of MF and the fusion of PCF, with the requirement of precise control, raise manufacturing complexity and fabrication cost. In Ref. [27], MF acts as a vector-dependent film, the injection of MF is simpler than the former, but there is still much room for improvement in simplifying the injection of MF. Therefore, magnetic field sensor with an improved performance, simple structure, low-cost, and an ability to measure both intensity and direction of the magnetic field is in demand.

In this paper, we report an all-fiber vector magnetic field sensor with two optical transmission channels based on interference detection. The sensor is established by tapering a capillary and two optical fibers simultaneously to form a dumbbell-like structure, which allows for the interaction between the evanescent field of the optical modes and magnetic fluid. Under an external magnetic field, an induced anisotropic distribution of magnetic nanoparticles (MNPs) at the interior capillary surface occurs and changes the phase of the interference spectrum of the two modes consequently. By observing chain-like aggregation of magnetic nanoparticles in a capillary, the vector-dependent effective refractive index (ERI) of the MF is explained. Compared with the previous works in magnetic field detection, we have achieved a breakthrough in extending the performance of magnetic field sensors from 2D planar to 3D space.

2. Principle and Fabrication

2.1 Observation of the Distribution of Nanoparticles in the Capillary

The RI of the MF depends on the microstructure of MNPs, which can be adjusted by the applied magnetic field [28], [29]. Analyzing the characteristics of MNPs from a micro perspective is of great significance for the structural design and performance evaluation of the MF-based optical fiber sensors. As shown in Fig. 1, an external magnetic field can incur the dynamic aggregation of nanoparticles in the capillary. The nanoparticles are rearranged and become oriented along the applied magnetic field, the rearrangement of nanoparticles consequently introduces anisotropy of MF inside the capillary. The nanoparticles are composed of a superparamagnetic core with magnetic moment mi and coated by a layer of surfactant. The aggregation between two nanoparticles forms by the magnetic dipole-dipole interactions. Chains and clusters are formed when the interaction is stronger than thermal disordering [29]. Significant changes in angle α and distance r between nanoparticles i and j indicate that the nanoparticles move to a new position by the induced magnetic force. According to the principle of fluid mechanics, the capillary structure locally changes the
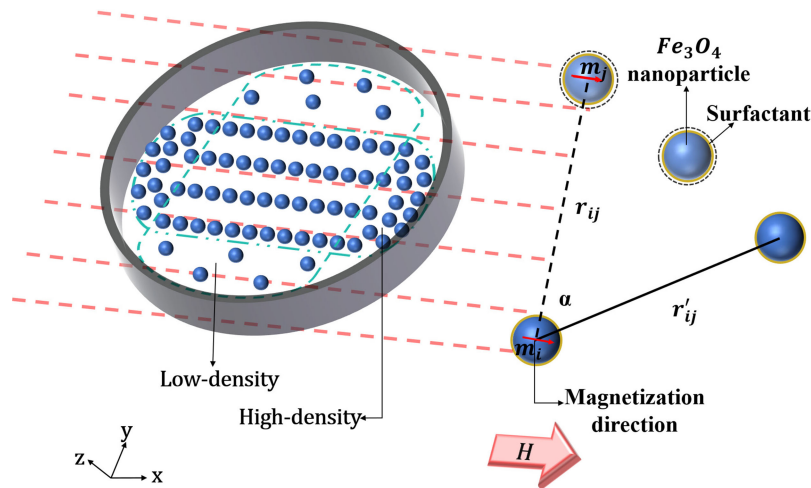
Fig. 1. A schematic view illustrating the anisotropic nano-chain cluster formation of Fe3O4 nanoparticles in a capillary and schematic diagram of dual-magnetic-dipole interactions under the magnetic field, r is the distance between two nanoparticles.
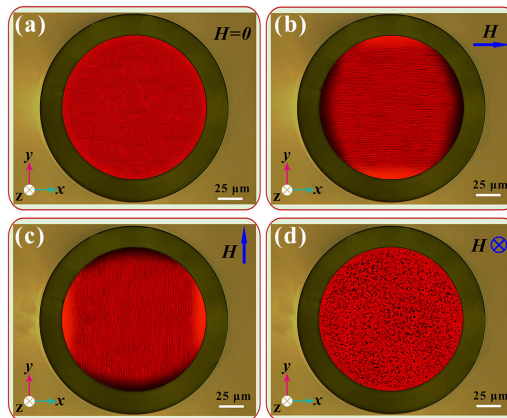
Fig. 2. Microscope images of the nanoparticles (a) without an external magnetic field. Anisotropic nanochain-clusters and dynamic aggregation of magnetic nanoparticles under different magnetic field directions (b) along the X-axis, (c) along the Y-axis, and (d) along the Z-axis.

magnetic moment of the magnetic nanoparticles and destroys the force balance of the MNPs. The new moment of a magnet will drive MNPs to form a chain cluster along the direction of the magnetic field. This results in an uneven density distribution of nanoparticles in the inner wall of the capillary.

A 10× objective lens of an optical microscope was used to observe the aggregation of MNPs in the capillary. The direction of the capillary axis was set along Z-axis and the cross-section in the X-Y plane. Note that the investigated MNPs are too small (~10 nm) to be captured by the optical microscopy, so that the MNPs with larger dimensions (200–300 nm) as alternatives were employed here for illustration purpose only. And one end of the quartz capillary with an inner diameter of 147 μm was spliced with a single-mode optical fiber. The capillary was then cut using an optical cutter, leaving approximately 200 μm of the quartz capillary, which acted as a sample pool. This sample pool with MF was connected to the light source through a single-mode optical fiber. As shown in Fig. 2(a), in the absence of an external magnetic field, the MNPs are distributed evenly and uniformly in the quartz capillary. Interestingly, as an external magnetic field is applied, agglomerations of the MNPs have been observed only near the sides of the capillary parallel
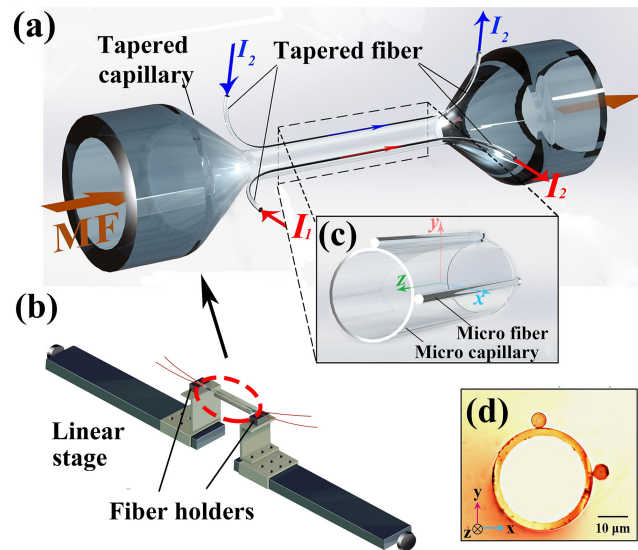
Fig. 3. (a) Schematic diagram of the sensor. (b) Linear stage for tapering and heating process. (c) An enlarged diagram of the taper region of the sensor. (d) Sectional microscope photograph of the sensor.

to the applied magnetic field, as shown in Figs. 2(b), (c) and (d). These figures also elucidate the dependency of the chain direction and MNPs density on the direction of the magnetic field. It can be immediately inferred that the directionally agglomerated MNPs on the inner wall of the capillary will change the ERI over this area, resulting in a shift in the detected transmission spectra. Therefore, this is an important characteristic that provides the opportunity of realizing the magnetic field vector sense.

2.2 Fabrication and Sensing Principle

The schematic diagram of the proposed sensor is shown in Fig. 3(a), where a section of tapered micro-capillary with its channel filled with MF is attached with two micro-fiber parallel to the cylinder axis. We proposed a concise process to fabricate the sensor with two 125 μm single-mode fibers and a quartz capillary with an outer diameter of 660 μm and a wall thickness of 65 μm, wherein the two fibers are arranged at an angle of 90° to each other along the outer wall of the capillary using UV-curing adhesive. Then the integrated structure was put on the flame of benzene lamp, both the two optical fibers and the capillary will soften gradually. With an appropriate tension at both ends by the linear stages, the optical fibers and the capillary will melt together during the heat and form a dumbbell-like structure. The linear stage shown in Fig. 3(b) were controlled by two motors with high precision. Figs. 3(c) and 3(d) are the enlarged schematic diagram and the cross-section microscope photograph of the dumbbell-like structure, respectively. The transverse geometry is almost unchanged over a length of 3 cm and it can be characterized by the following parameters: capillary outer diameter D = 41.5 μm, wall thickness t = 2.5 μm, and the attached fibers in the X-direction and Y-direction, respectively, have diameters of 4.8 μm and 5.2 μm. I1 and I2 are the intensity of transmitted light in two channels respectively. After the thermal stretch, MF (EMG 900, Ferrotec Inc.) is injected from one end of the quartz capillary and encapsulated inside it, and the diameter of the MNPs interspersed in the MF is 10 nm. In addition, the uneven heating can occur in fused biconical taper molding. These reasons together led to diameter differences between the two microfibers around the capillary. The loss and half height width exhibited some differences between the two channels as seen by an interference dip in the transmission spectra, but there are few differences in the wavelength of interferometric dips between the spectra of the two channels.
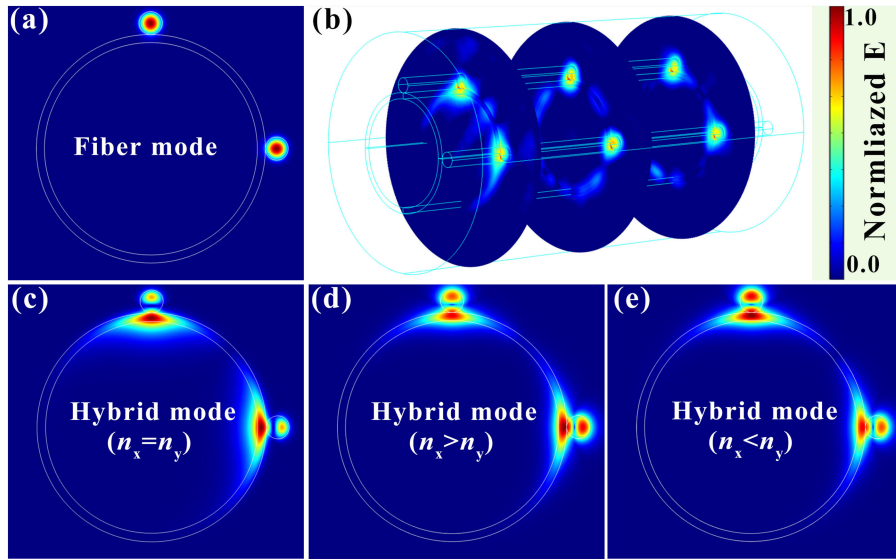
Fig. 4. The finite element simulation model of the sensor. (a) fiber mode, (b) a hybrid mode in three-dimension mode. The power of the hybrid mode distributed in the optical fiber and the capillary wall varies with the ERI along the X and Y directions, (c) when $n_x = n_y$, the power of the hybrid mode along X direction is equivalent to the Y-direction, (d) when $n_x > n_y$ and (e) $n_x < n_y$, the power distribution of the hybrid mode is a direction-dependent variable.

Therefore, in our magnetic detecting experiment, the spectra of these two channels can be used as reference for each other.

As light propagates through the two tapered fibers, two discrete optical modes coexisting in each fiber arm are defined as a fiber mode and a hybrid mode by the path of light propagation [28]. The fiber mode only propagates inside the guiding fibers, as shown in Fig. 4(a), while the hybrid mode propagating through both fibers and wall of the capillary, as shown in Fig. 4(c)–(e). These two discrete modes will interfere with each other at the end of the tapered structure and form an interference spectrum eventually. The transmission of the sensor can be expressed as [29]–[31]:

$$I = I_{fib} + I_{hyb} + 2\sqrt{I_{fib} \cdot I_{hyb}} \cos\left(\frac{2\pi L \, \Delta n_{eff}}{\lambda}\right) \tag{1}$$

where I_{fib} and I_{hyb} are the intensities of the fiber mode and the hybrid mode, Δn_{eff} is the effective refractive index difference of the fiber mode and the hybrid mode. L is the length of the interference region. The attenuation dip wavelength of the spectrum in a single channel can be express as [29]–[31]:

$$\lambda_n = \frac{2\Delta n_{eff} L}{2n + 1} \tag{2}$$

where n is the interference order, the RI of the MF in the micro-capillary can be modulated by an external magnetic field [32], based on the localized aggregation of MNPs discussed in Section 2.1, and then the ERI of the hybrid mode will be changed then Δn_{eff} will be changed correspondingly.

The effect of direction changes on the magnetic field measurements was also simulated by using COMSOL MULTIPHYSICS. As shown in Fig. 4(a), the finite element model (FEM) was obtained by solving the wave equation and calculating the electric field intensity distribution over the cross-section, the fiber mode mainly exists in the fiber. Fig. 4(b) illustrates that the intensities of the fiber mode and the hybrid mode are uniform along the radial direction of the microfiber. When an external magnetic field is applied, the MNPs-mixed MF becomes an anisotropic medium, and the intensity of the two hybrid modes turns out to be differentiable. Moreover, such intensity discrepancy
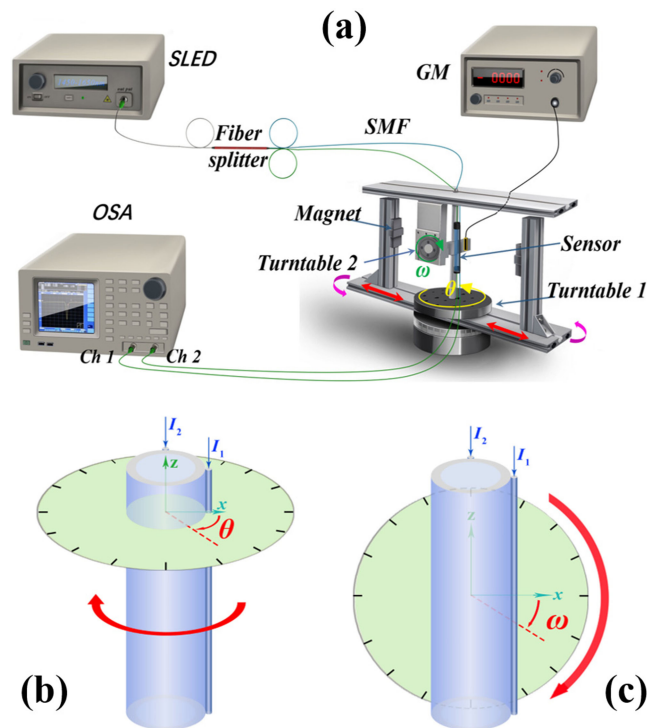
Fig. 5. (a) Experimental setup. (b) Magnetic field direction rotation θ. (c) Sensor axis rotation ω.

varies according to the different directions of the magnetic field, as shown in Figs. 4(c), 4(d) and 4(e). These simulated results certainly confirm our aforementioned assumption that the hybrid mode has the capability to quantitatively reflect both intensity and direction of the magnetic field.

3. Experiment and Discussion

The experimental setup for the magnetic field measurement is illustrated in Fig. 5(a). A light beam emanated by a superluminescent light-emitting diode (SLED) with a spectral range from 1450 nm to 1650 nm was divided into two beams by a fiber splitter. These two beams were launched into the X and Y channels of the sensor respectively, and their transmission spectra were recorded by an optical spectrum analyzer (OSA, Yokogawa, AQ6370C, covering a spectral range from 1250 to 1650 nm, with a resolution of 0.02 nm) in real-time. Moreover, the magnetic field control instrument (MFCI, customized from Sichuan Zhiyan Technology Co., Ltd.) was used as the magnetic field source, the intensity of the magnetic field can be precisely controlled by adjusting the distance between two magnets. Turntable 1 and turntable 2 mounted with the magnetic field device were used to adjust the direction of the magnetic field and the direction of the sensor, respectively. The angle between X-channel and the direction of the magnetic field is defined as θ, which is controlled by the turntable 1. The angle between the sensor axis and the Z-axis is defined as ω, which is controlled by the turntable 2. And details of these two turntables are shown in Figs. 5(b) and 5(c). During the experiment, the sensor was fixed with glue in the area as shown in the figure, which ensures that the sensor is always in a uniform magnetic field while avoiding fluctuations in the spectrum caused by bending of the sensor area. We used a Gaussian meter (GM) with a resolution of 0.1 mT to measure the intensity of the magnetic field.

We first studied the response of the sensor to the intensity of the magnetic field, as the direction of the magnetic field is fixed on the X-axis. When the external magnetic field intensity is 0 mT, the transmission spectrum and wavelength shift responses are shown in Fig. 6(a), and the transmission trough at 1543 nm can be used for wavelength detection (the rectangular area of black dotted line).
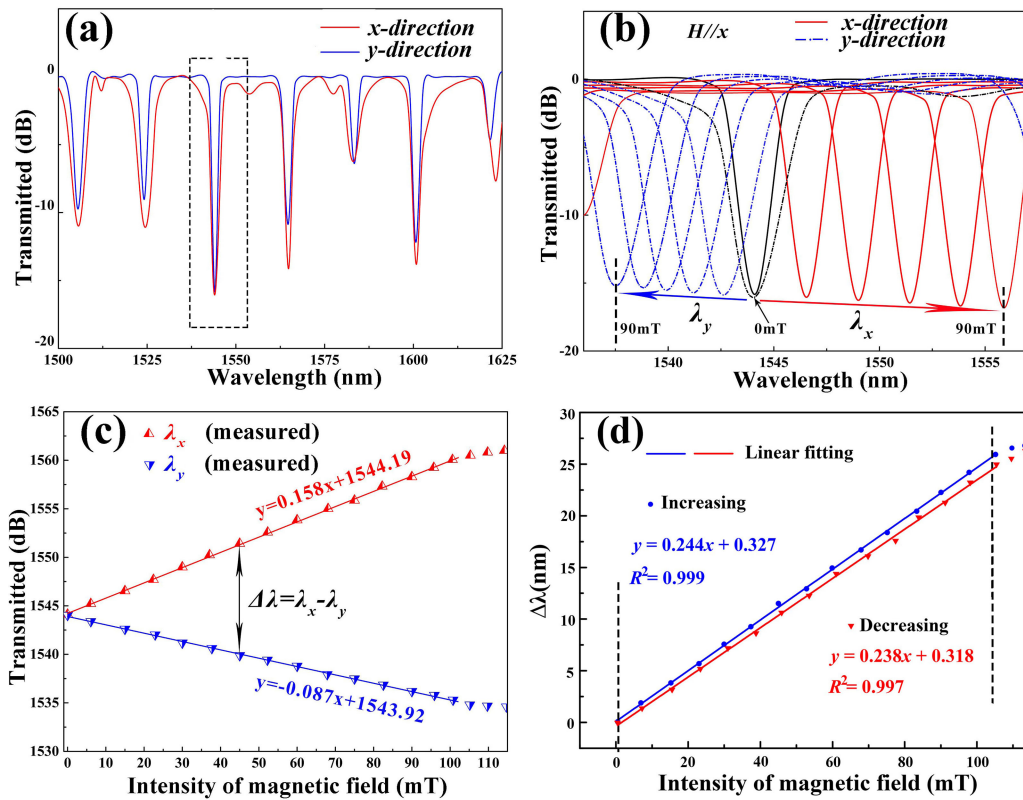
Fig. 6. (a) Transmission spectra of the sensor when the magnetic field intensity is 0 mT. (b) Transmission spectra corresponding to different magnetic field intensity. (c) The shift of the transmission troughs varies with magnetic field intensity in the two channels are 158 pm/mT and −87 pm/mT. (d) Wavelength shift as a function of magnetic intensity applied in increasing and decreasing directions.

Fig. 6(b) demonstrates that the phase shift due to the varying intensity of magnetic field can be easily quantified by positioning the transmission troughs of the X- and Y-channels defined as λ_x and λ_y, respectively. And then, the wavelength shift $\Delta\lambda$, defined as the difference of the shifts between the X- and Y-channels, has been used to characterize the sensor and expressed as:

$$\Delta\lambda = \lambda_x - \lambda_y \tag{3}$$

Based on this characterization, the change of the magnetic field can be monitored by tracking the wavelength shift of the two channels synchronously. With increasing the magnetic field intensity by gradually adjusting the distance between the two NdFeB magnets, more and more MNPs are removed from the Y direction while being agglomerated on the X direction. This leads to a redshift of the transmission troughs for the X-channel [red curves in Fig. 6(b)] while a blue shift for the Y-channel [blue curves in Fig. 6(b)]. The transmission trough shifts of both channels show good linearity can be expressed as a function of intensity (H). As shown in Fig. 6(c) the slope of λ_x and λ_y are 158 pm/mT and −87 pm/mT, respectively, indicating that the anisotropic behavior of the MF in the capillary takes place on exposure to the external magnetic field. The above findings are consistent with the simulation results. As more and more nanoparticles gather into chains in the capillary, the refractive index of this region will increase. This will lead to a larger phase difference between fiber mode and hybrid mode. Due to the hysteresis and saturation of the MF [33], each data point was recorded after changing the magnetic field for 5 minutes. As illustrated in Fig. 6(d), with the increase and decrease of the magnetic field intensity, the experimental data shows good
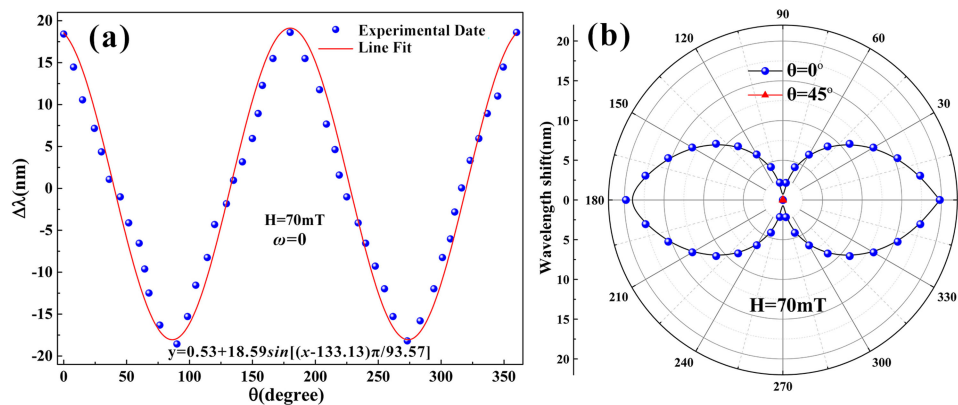
Fig. 7. In the magnetic field with an intensity of 70 mT. (a) spectra response to θ changes from 0° to 90° and 90° to 180°. (b) The dynamic response curves at different $\theta = 0°$ and 45° varies with ω (0°−360°).

linearity in the range of 0–90 mT. Because of the hysteresis effect mentioned above, the fitting curve of wavelength shift moves downward slightly when the intensity of magnetic field decrease.

In addition to the magnetic field intensity measurement, an investigation on the directional sensitivity of the sensor was implemented. During the magnetic field direction experiment, the sensor axis was perpendicular to the direction of the magnetic field ($\omega = 0°$) and the intensity of the magnetic field was fixed at 70 mT. According to the Eq. (2), the wavelength shift $\Delta\lambda$ was analyzed and fitted with the sinusoidal function as shown in Fig. 7(a). When the angle between the direction of the magnetic field and the X-channel increases from 0° to 90° the wavelength shift changes from 18 nm to −18 nm, and when 90°< θ < 180°, it then returns to 18 nm again from −18 nm. In this cycle, with the change of magnetic field direction, wavelength shift is a good indicator of the variation of MF distribution in the capillary. In order to further evaluate the performance of the sensor, a series of studies were conducted in the direction of the sensor. By rotating the sensor from 0° to 360°, the response curves to the rotation angle have been characterized. As shown in Fig. 7(b), for constant magnetic field intensity, transmission curves can be well fitted with a polar equation, and the two pairs of symmetric response peaks appear in the two orthogonal directions of the response curves. The response peak reflects the anisotropic aggregation of nanoparticles in the capillary. Specifically, the position of the peak can indirectly characterize the location of the nanoparticles in the capillary. In the case of the magnetic field with a direction of 45° (or 135°), the densities of nanoparticles near both X- and Y-channel are identical, the wavelength shift thereby is always kept 0 over a full rotation of the angle ω (0°−360°). This means that the magnetic field with 45° makes the wavelength shift independent of the angle ω. Per the experimental observations, the direction information of an unknown magnetic field can be measured by two steps. Note that the impact of the temperature fluctuations of about 1 °C in our experiment is trivial so that the temperature effect is not considered here.

4. Conclusions

In conclusion, a compact fiber-optic vector magnetic field sensor with two optical transmission channels based on the interference of the fiber mode and the hybrid mode is proposed and experimentally demonstrated. Taking advantage of the anisotropic distribution of MNPs at the capillary interior surface, such a magnetic field sensor is capable to measure both magnetic field intensity and direction simultaneously. The experimental results show that the sensitivity of 244.0 pm/mT can be achieved, and the direction error is only ±1.4°. In addition, the proposed vector magnetic field sensor with such high sensitivity and simple structure as well as compact dimensions shows great advantages in magnetic field detection in 3D space. We are working hard to improve the structure of the sensor, aiming to explore its further potential in the future vector magnetic field measurement.

References

[1] B. Lee, S. Roh, and J. Park, "Current status of micro- and nano-structured optical fiber sensors," *Opt. Fiber Technol.*, vol. 15, no. 3, pp. 209–221, 2009.

[2] N. Alberto, M. Domingues, P. André, and P. Antunes, "Optical fiber magnetic field sensors based on magnetic fluid: A review," *Sensors*, vol. 18, no. 12, p. 4325, 2018.

[3] Y. Shi, Y. Ma, and Y. Wang, "Magneto-elastic-optical coupling of Terfenol-D based optical fiber magnetic field sensors," *Mater. Res. Exp.*, vol. 6, no. 8, p. 086106, May 2019.

[4] M. Yang, J. Dai, C. Zhou, and D. Jiang, "Optical fiber magnetic field snesors with TbDyFe magnetostrictive thin films as sensing materials," *Opt. Exp.*, vol. 17, no. 23, pp. 20777–20782, Oct. 2009.

[5] H. Horng, C. Hong, and H. Yang, "Novel properties and applications in magnetic fluids," *J. Phys. Chem. Solids*, vol. 62, no. 9, pp. 1749–1764, Jan. 2001.

[6] Y. Zhao, X. Liu, Y. N. Lv, and Q. Wang, "Review on optical fiber sensors based on the refractive index tunability of ferrofluid," *J. Lightw. Technol.*, vol. 35, no. 16, pp. 3406–3412, Jun. 2017.

[7] P. Zu *et al.*, "Enhancement of the sensitivity of magneto-optical fiber sensor by magnifying the birefringence of magnetic fluid film with Loyt-Sagnac interferometer," *Sens. Actuators B.*, vol. 191, pp. 19–23, Feb. 2014.

[8] A. Mahmood, V. Kavungal, S. Ahmed, G. Farrell, and Y. Semenova, "Magnetic-field sensor based on whispering-gallery modes in a photonic crystal fiber infiltrated with magnetic fluid," *Opt. Lett.*, vol. 40, no. 21, pp. 4983–4986, Nov. 2015.

[9] R. Gao, Y. Jiang, and S. Abdelaziz, "All-fiber magnetic field sensors based on magnetic fluid-filled photonic crystal fibers," *Opt. Lett.*, vol. 38, no. 9, pp. 1539–1541, May. 2014.

[10] L. Luo, S. Pu, J. Tang, X. Zeng, and M. Lahoubi, "Highly sensitive magnetic field sensor based on microfiber coupler with magnetic fluid," *Appl. Phys. Lett.*, vol. 106, no. 19, p. 193507, May 2015.

[11] J. Wu *et al.*, "Magnetic-field sensor based on core-offset tapered optical fiber and magnetic fluid," *J. Opt.*, vol. 16, p. 075705, Jun. 2014.

[12] F. Wei *et al.*, "Magnetic field sensor based on a combination of a microfiber coupler covered with magnetic fluid and a Sagnac loop," *Sci. Rep.*, vol. 7, p. 4725, Jul. 2017.

[13] X. Zhou, X. Li, S. Li, G. An, and T. Cheng, "Magnetic Field sensing based on SPR optical fiber sensor interacting with magnetic fluid," *IEEE Trans. Instrum. Meas.*, vol. 68, no. 1, pp. 234–239, Jan. 2019.

[14] Z. Tong, Y. Wang, W. Zhang, and P. Luan, "Optical fiber magnetic field sensor based on multi-mode fiber and core-offset structure," *J. Mod. Opt.*, vol. 64, no. 12, pp. 1129–1133, 2017.

[15] W. Bao, X. Qiao, Q. Rong, and F. Chen, "Fiber-Optic vector magnetometer based on magnetic fluid and fiber bragg grating written on a Multi-Clad Fiber," *IEEE. SENS. J.*, vol. 18, no. 18, pp. 7486–7491, Sep. 15, 2018.

[16] J. Zheng, X. Dong, P. Zu, J. Ji, H. Su, and P. Shum, "Intensity-modulated magnetic field sensor based on magnetic fluid and optical fiber gratings," *Appl. Phys. Lett.*, vol. 103, no. 18, p. 183511, Oct. 2013.

[17] D. Yang *et al.*, "Magnetic field sensing based on tilted fiber Bragg grating coated with nanoparticle magnetic fluid," *Appl. Phys. Lett.*, vol. 104, no. 6, p. 061903, Jan. 2014.

[18] Z. Zhang *et al.*, "Plasmonic fiber-optic vector magnetometer," *Appl. Phys. Lett.*, vol. 108, no. 10, p. 101105, Feb. 2016.

[19] J. Wu *et al.*, "Low-temperature sensitive intensity interrogated magnetic field sensor based on modal interference in thin-core fiber and magnetic fluid," *Appl. Phys. Lett.*, vol. 104, no. 25, p. 252402, Jun. 2014.

[20] R. Lv, Y. Zhao, D. Wang, and Q. Wang, "Magnetic Fluid-Filled optical fiber Fabry–Pérot sensor for magnetic field measurement," *IEEE Photonics Technol. Lett.*, vol. 26, no. 3, pp. 217–219, Feb. 2014.

[21] T. Yao, S. Pu, J. Rao, and J. Zhang, "Investigation of optical force on magnetic nanoparticles with magnetic-fluid-filled Fabry-Perot interferometer," *Sci. Rep.*, vol. 8, p. 12352, Aug. 2018.

[22] X. Li, R. Ma, and Y. Xia, "Magnetic field sensor exploiting light polarization modulation of microfiber with magnetic fluid," *J. Lightw. Technol.*, vol. 36, no. 9, pp. 1620–1625, May 2018.

[23] P. Zu, C. Chan, T. Gong, Y. Jin, W. Wong, and X. Dong, "Magneto-optical fiber sensor based on bandgap effect of photonic crystal fiber infiltrated with magnetic fluid," *Appl. Phys. Lett.*, vol. 101, no. 24, p. 241118, Nov. 2012.

[24] J. Cui, D. Qi, H. Tian, and H. Li, "Vector optical fiber magnetometer based on capillary filled with magnetic fluid," *Appl. Opt.*, vol. 58, no. 10, pp. 2754–2760, Apr. 2019.

[25] Z. Jiang *et al.*, "High-sensitivity vector magnetic field sensor based on side-polished fiber plasmon and ferrofluid," *Opt. Lett.*, vol. 43, no. 19, pp. 4743–4746, Sep. 2018.

[26] J. Yin *et al.*, "All-fiber-optic vector magnetometer based on nano-magnetic fluids filled double-clad photonic crystal fiber," *Sens. Actuators B, Chem.*, vol. 238, pp. 518–524, Jul. 2017.

[27] J. Yin *et al.*, "All-fiber-optic vector magnetometer based on anisotropic magnetism-manipulation of ferromagnetism nanoparticles," *Appl. Phys. Lett.*, vol. 101, no. 23, p. 231104, Jun. 2017.

[28] G. Bertoni, B. Torre, A. Falqui, D. Fragouli, A. Athanassiou, and R. Cingolani, "Nanochains formation of superparamagnetic nanoparticles," *J. Phys. Chem. C.*, vol. 115, no. 15, pp. 7249–7254, Mar. 2011.

[29] S. V. Kredentser, M. M. Kulyk, V. Kalita, K. Y. Slyusarenko, V. Y. Reshetnyak, and Y. A. Reznikov, "Magneto-induced anisotropy in magnetic colloids of superparamagnetic magnetite nanoparticles in an external magnetic field," *Soft Matter*, vol. 13, no. 22, pp. 4080–4087, May 2017.

[30] L. Liang, L. Jin, Y. Ran, L. Sun, and B. Guan, "Interferometric detection of microRNAs using a capillary optofluidic sensor," *Sens. Actuators B, Chem.*, vol. 242, pp. 999–1006, Sep. 2017.

[31] L. Liang, L. Jin, Y. Ran, L. Sun, and B. Guan, "Fiber Light-Coupled optofluidic waveguide (FLOW) immunosensor for highly sensitive detection of p53 protein," *Anal. Chem.*, vol. 90, pp. 10857–10857, Aug. 2018.

[32] Z. Ma, Y. Miao, Y. Li, H. Zhang, B. Li, Y. Cao, and J. Yao, "A highly sensitive magentic field sensor based on a tapered microfiber," *IEEE Photon. J.*, vol. 10, no. 4, Aug. 2018.

[33] Z. Li *et al.*, "Ultrasensitive magnetic field sensor based on an in-fiber Mach–Zehnder interferometer with a magnetic fluid component," *Photon. Res.*, vol. 4, no. 5, pp. 197–201, Sep. 2016.

[34] C. Hong, S. Yang, H. Horng, and H, Yang, "Control parameters for the tunable refractive index of magnetic fluid films," *J. Appl. Phys.*, vol. 94, no. 6, pp. 3849–3853, Jun. 2003.